

---

This is an electronic reprint of the original article.  
This reprint may differ from the original in pagination and typographic detail.

Horsten, Niels; Groth, Mathias; Dekeyser, Wouter; Van Uytven, Wim; Carli, Stefano; JET Contributors

## Combination of micro-macro and spatially hybrid fluid-kinetic approach for hydrogenic plasma edge neutrals

*Published in:*  
Contributions to Plasma Physics

*DOI:*  
[10.1002/ctpp.202100188](https://doi.org/10.1002/ctpp.202100188)

Published: 01/06/2022

*Document Version*  
Publisher's PDF, also known as Version of record

*Published under the following license:*  
CC BY-NC-ND

*Please cite the original version:*  
Horsten, N., Groth, M., Dekeyser, W., Van Uytven, W., Carli, S., & JET Contributors (2022). Combination of micro-macro and spatially hybrid fluid-kinetic approach for hydrogenic plasma edge neutrals. *Contributions to Plasma Physics*, 62(5-6), Article 202100188. <https://doi.org/10.1002/ctpp.202100188>

---

This material is protected by copyright and other intellectual property rights, and duplication or sale of all or part of any of the repository collections is not permitted, except that material may be duplicated by you for your research use or educational purposes in electronic or print form. You must obtain permission for any other use. Electronic or print copies may not be offered, whether for sale or otherwise to anyone who is not an authorised user.

# Combination of micro–macro and spatially hybrid fluid-kinetic approach for hydrogenic plasma edge neutrals

Niels Horsten<sup>1</sup> | Mathias Groth<sup>1</sup> | Wouter Dekeyser<sup>2</sup> | Wim Van Uytven<sup>2</sup> | Stefano Carli<sup>2</sup> | JET Contributors

<sup>1</sup>Department of Applied Physics, Aalto University, Aalto, Finland

<sup>2</sup>Department of Mechanical Engineering, KU Leuven, Leuven, Belgium

## Correspondence

Groth Mathias, Department of Applied Physics, Aalto University, Aalto FI-00076, Finland.

Email: [mathias.groth@aalto.fi](mailto:mathias.groth@aalto.fi)

## Funding information

Euratom, Grant/Award Number: 633053

## Abstract

A new hybrid fluid-kinetic approach for the hydrogenic neutrals (atoms and molecules) in the plasma edge is presented. The hybrid approach combines a fully kinetic model for the atoms in the low-collisional regions near the vessel wall, and for the molecules in the whole plasma edge domain, with a micro–macro approach for atoms originating from recycling at the divertor targets, volumetric recombination, and dissociation of molecules. With the micro–macro approach, the originally scattering-dominated collision term due to charge-exchange collisions in the kinetic equation is transformed to an absorption-dominated term, while a large part of the neutral population is treated through a fluid approach. For JET L-mode plasmas, the premature termination of Monte Carlo particle trajectories in the hybrid approach leads to a reduction of the CPU time by approximately a factor 3 for a high-recycling case and by approximately a factor 11 for a partially detached case compared with a simulation with fully kinetic neutrals and the same amount of particles. For coupled fluid plasma – hybrid neutral simulations – the hybrid approach predicts the plasma divertor target profiles with a maximum hybrid-kinetic discrepancy of approximately 30%.

## KEYWORDS

fluid approximation, kinetic model, neutrals, plasma edge modelling

## 1 | INTRODUCTION

In contrast to the charged species (ions and electrons) in the plasma edge of magnetic-confinement nuclear fusion devices, for which in general a fluid approximation is used,<sup>[1]</sup> both kinetic and fluid models are in use for the neutral hydrogenic particles (atoms and molecules). On the one hand, a kinetic approach, typically solved with a Monte Carlo (MC) method,<sup>[2]</sup> is generally valid for all shapes of underlying particle-velocity distributions, but becomes computationally costly for high-collisional cases. On the other hand, fluid models are usually solved deterministically

JET Contributors: See the author list of ‘Overview of JET results for optimising ITER operation’ by J. Mailloux et al. to be published in Nuclear Fusion Special issue: Overview and Summary Papers from the 28th Fusion Energy Conference (Nice, France, 10–15 May 2021).

This is an open access article under the terms of the Creative Commons Attribution-NonCommercial-NoDerivs License, which permits use and distribution in any medium, provided the original work is properly cited, the use is non-commercial and no modifications or adaptations are made.

© 2022 The Authors. *Contributions to Plasma Physics* published by Wiley-VCH GmbH.

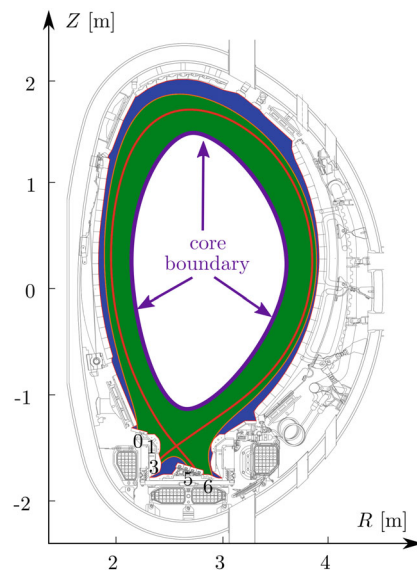


**FIGURE 1** Poloidal cross-section of JET tokamak: the green and blue areas correspond to the plasma fluid domain and the void/vacuum regions, respectively. The relevant target tile numbers are indicated. In our plasma grid, the step between tiles 5 and 6 is less steep. Figure based on fig. 1 in Reference [6]

and are computationally much cheaper, but they are often inaccurate,<sup>[3–5]</sup> with discrepancies with simulations with fully kinetic neutrals that easily become larger than 50% in the divertor region.<sup>[6]</sup>

There are two main issues for a purely fluid neutral description: (i) there are low-collisional regions where the hydrogenic atom velocity distribution deviates significantly from a Maxwellian equilibrium distribution; and (ii) even if the hydrogenic atoms reach the fluid limit in certain regions, the fluid limit is in general not valid for the hydrogenic molecules. Due to issue (ii), there is typically no explicit treatment of molecules in the fluid neutral models of most plasma edge codes. Especially in the outermost regions where the plasma density approaches zero, the atom velocity distribution deviates significantly from a Maxwellian distribution. Hence, it is recommended to use a fully kinetic model in the outermost regions. This is accomplished with the spatially hybrid approach from Blommaert et al.,<sup>[7]</sup> where a distinction is made between the plasma grid region (in which the plasma fluid equations are solved) and the so-called void or vacuum regions between the outermost simulated flux surfaces and the real vessel wall (see Figure 1). A fluid model for the hydrogenic atoms in the plasma grid (green region in Figure 1) is coupled to a kinetic model for the atoms in the void regions (blue regions in Figure 1). In Reference [6], the model is extended with a coupling to a fully kinetic model for the molecules (and possibly also for the impurities) in the whole domain to resolve issue (ii). Although the kinetic treatment of atoms in the void regions reduces the discrepancies with the fully kinetic model significantly, there are still other regions within the plasma grid where the hydrogenic atoms do not reach the fluid limit. These additional regions are case specific and it is infeasible to distinguish them in advance.

To correct for errors from the fluid atom model in the plasma grid region without the need for a user-defined criterion to determine the fluid and kinetic regions, a micro–macro approach has been developed.<sup>[8]</sup> However, this method has only been assessed for a very simplified rectangular slab case without void regions and molecules, and assuming a fixed plasma background. In this contribution, we combine the spatially hybrid and micro–macro approach to simulate realistic geometries including the coupling to kinetic molecules and fluid plasma. The method is implemented in the newly developed unstructured version of the SOLPS-ITER code suite,<sup>[9]</sup> which consists of the B2.5 code for the fluid species (ions, electrons, and fluid neutrals) and the EIRENE code for the kinetic neutrals.<sup>[2]</sup> Due to the use of a nine-point stencil, proper numerical treatment for non-orthogonal grids is addressed, which becomes essential for the isotropic fluid neutrals.<sup>[10]</sup>

## 2 | FULLY KINETIC MODEL

Firstly, we formulate the fully kinetic model for the hydrogenic atoms. In this publication, we only consider a purely hydrogenic plasma with a single isotope consisting of ions, atoms, and molecules. However, the framework for the neutrals

is easily extended with a coupling to the impurity species. The hybrid model equations are derived in Section 3 starting from the fully kinetic description. Whereas the theoretical model is described for a general geometry in Sections 2 and 3, we only apply it to a 2D tokamak geometry in Section 4.

The steady-state kinetic (Boltzmann) equation for the atom position–velocity phase–space distribution  $f_a(\mathbf{r}, \mathbf{v})$  can be written as follows:

$$\mathbf{v} \cdot \nabla f_a(\mathbf{r}, \mathbf{v}) = S_a(\mathbf{r}, \mathbf{v}) + Q_a(f_a(\mathbf{r}, \mathbf{v})), \quad (1)$$

with  $\mathbf{r}$  and  $\mathbf{v}$  the position and particle-velocity vector, respectively, and  $\nabla$  the gradient with respect to the position. The source term  $S_a(\mathbf{r}, \mathbf{v})$  contains sources from volumetric recombination, dissociation of molecules, and ion recycling (as fast atoms) at the boundaries. The collision term  $Q_a(f_a(\mathbf{r}, \mathbf{v}))$  consists of ionization and charge-exchange events:

$$Q_a(f_a(\mathbf{v})) = -n_e K_i f_a(\mathbf{v}) + \int_{\mathbf{v}'} \sigma_{cx} \left( \frac{m}{4} \|\mathbf{v} - \mathbf{v}'\|^2 \right) \|\mathbf{v} - \mathbf{v}'\| (f_i(\mathbf{v}) f_a(\mathbf{v}') - f_i(\mathbf{v}') f_a(\mathbf{v})) d\mathbf{v}', \quad (2)$$

where  $m$  refers to atom particle mass,  $n_e$  refers to electron density,  $f_i(\mathbf{v})$  refers to ion position–velocity phase–space distribution (which is assumed to be a drifting Maxwellian),  $K_i$  refers to ionization rate coefficient, and  $\sigma_{cx}$  refers to charge-exchange microscopic cross-section as a function of the centre-of-mass kinetic energy. The charge-exchange term in Equation (2) contains the integral over the whole velocity space  $\int_{\mathbf{v}'} \dots d\mathbf{v}'$ . Including neutral–neutral collisions in the models is out of the scope of this paper, but we briefly discuss their impact on the model equations in Section 3.4. In Equation (2) (and in other equations in this publication), we omit the explicit notation of the position dependency.

To simplify the micro–macro model equations in Section 3.2, an approximate expression for the collision term is used:

$$Q_a(f_a(\mathbf{v})) \approx -n_e K_i f_a(\mathbf{v}) + K_{cx,m} (n_a f_i(\mathbf{v}) - n_i f_a(\mathbf{v})), \quad (3)$$

with  $n_a \triangleq \int_{\mathbf{v}} f_a(\mathbf{v}) d\mathbf{v}$  and  $n_i \triangleq \int_{\mathbf{v}} f_i(\mathbf{v}) d\mathbf{v}$  the atom and ion density, respectively. Equation (3) makes use of the momentum-linearized charge-exchange rate coefficient, which is defined in Reference [11] to obtain approximately the same momentum source as with the original expression in Equation (2). Reference [11] contains a detailed evaluation of the momentum source from the momentum-linearized rate coefficient approximation. The influence on the resulting plasma state is assessed in Section 4.2.

The hydrogenic molecules are still treated fully kinetically in the hybrid approach. The considered molecular processes can be found in Reference [6]. The fully kinetic approach allows to easily add new molecular processes.

### 3 | FROM KINETIC TO COMBINED SPATIALLY–MICRO–MACRO HYBRID NEUTRAL MODEL

The combined spatially–micro–macro model is obtained by splitting up the atom particle-velocity distribution  $f_a(\mathbf{r}, \mathbf{v})$  into two steps.

#### 3.1 | Step 1: spatial decomposition

The spatial decomposition is based on the different types of sources and exploits the stratified source sampling technique in EIRENE<sup>[2]</sup>, that is, the total source  $S_a(\mathbf{r}, \mathbf{v})$  is split into different independent strata based on the source type and location. We write the total atom source  $S_a(\mathbf{r}, \mathbf{v})$  as

$$S_a(\mathbf{r}, \mathbf{v}) = S_a^k(\mathbf{r}, \mathbf{v}) + S_a^{mM}(\mathbf{r}, \mathbf{v}), \quad (4)$$

with  $S_a^k$  containing all strata that are treated fully kinetically and  $S_a^{mM}$  containing the strata for which the micro–macro approach is used.

Exploiting the linearity of the fully kinetic equation (Equation (1)), the total atom velocity distribution  $f_a(\mathbf{r}, \mathbf{v})$  can be similarly decomposed as follows:

$$f_a(\mathbf{r}, \mathbf{v}) = f_a^k(\mathbf{r}, \mathbf{v}) + f_a^{\text{mM}}(\mathbf{r}, \mathbf{v}), \quad (5)$$

with  $f_a^k$  and  $f_a^{\text{mM}}$  following from

$$\mathbf{v} \cdot \nabla f_a^k(\mathbf{r}, \mathbf{v}) = S_a^k(\mathbf{r}, \mathbf{v}) + Q_a(f_a^k(\mathbf{r}, \mathbf{v})), \quad (6)$$

$$\mathbf{v} \cdot \nabla f_a^{\text{mM}}(\mathbf{r}, \mathbf{v}) = S_a^{\text{mM}}(\mathbf{r}, \mathbf{v}) + Q_a(f_a^{\text{mM}}(\mathbf{r}, \mathbf{v})), \quad (7)$$

respectively. A fully kinetic MC approach is still used for Equation (6), whereas the micro–macro approach described in Section 3.2 is used for Equation (7). As implemented in this way, source strata for which a fully kinetic treatment is required (e.g., to model the transport in the void regions) and strata for which the micro–macro approach becomes inefficient due to long particle mean free paths<sup>[8]</sup>, can still be treated fully kinetically.

For the spatial decomposition, we define an interface that distinguishes between the micro–macro and fully kinetic regions. This interface is located at flux surfaces in the far scrape-off layer and far private-flux regions, where the plasma density becomes very low. For standard SOLPS-ITER simulations, the plasma fluid grid does not extend up to the real vessel wall, as illustrated in Figure 1. It is convenient to make the micro–macro–kinetic interface coincide with the already existing plasma-void interfaces. However, when the plasma fluid grid covers the whole domain up to the real vessel wall, such as in simulations with SOLEDGE2D<sup>[12]</sup> and possibly with the extended grid version of SOLPS-ITER,<sup>[9]</sup> it is less clear which flux surfaces need to be selected for an optimal trade-off between accuracy and computational cost. As future work, it is recommended to develop an automated procedure to determine the location of the interface based on the local Knudsen number (defined as the ratio of the local charge-exchange mean free path and a characteristic macroscopic length scale) averaged over the flux surface. References [13,14] both show that a fluid model for the plasma edge atoms becomes valid for Knudsen numbers smaller than 1.

Two types of strata are kept in the fully kinetic part  $S_a^k$ :

1. Recycling of ions at the outermost flux surfaces: In standard SOLPS-ITER simulations, it is typically assumed that ions recycle already at the plasma-void interfaces instead of at the real vessel wall. Although we also assume in this paper ion recycling at the plasma-void interfaces, the spatial decomposition can be applied as well when assuming recycling at the real vessel wall. An incident ion has a certain probability to be recycled as an atom or thermally released as a molecule, which is, for example, determined by the TRIM code database.<sup>[15]</sup> Due to the possible long mean free path near these regions, the micro–macro approach becomes inefficient and the computational cost of a fully kinetic approach is already sufficiently low for this type of strata.
2. Fluid atoms sampled at the micro–macro–kinetic interfaces and sent into the fully kinetic regions. To correctly model the transport in the fully kinetic regions, atoms from the micro–macro model reaching the fully kinetic regions are transferred from the micro–macro distribution ( $f_a^{\text{mM}}$ ) to the fully kinetic part. This type of strata makes that in fact  $S_a^k$  also depends on  $f_a^{\text{mM}}$ , which is omitted in the notation of Equations (4) and (6).

For both types of strata in  $S_a^k$ , the particles are followed in the MC simulation until they ionize or hit a (partially) absorbing surface (pump or core boundary).

Then, the source/sink  $S_a^{\text{mM}}$  contains the remaining contributions:

- Recycling of ions as atoms at the divertor targets (source).
- Volumetric recombination (source).
- Dissociation of molecules (source).
- (Micro–macro) atoms flying from the plasma grid region into the fully kinetic regions (sink). This term compensates for the source of atoms sampled at the micro–macro–kinetic interfaces (type 2 of strata in  $S_a^k$ , enforcing Equation (4)).

### 3.2 | Step 2: micro–macro decomposition

For the purely spatially hybrid method of Reference [6], the fully kinetic model in Equation (6) was coupled to a fully kinetic model for the molecules and a purely fluid model for the atoms inside the plasma grid (green region in Figure 1). In Reference [6], there were two approaches for the treatment of atoms resulting from molecular dissociation: (i) treating them as a fluid; or (ii) treating them fully kinetically. When comparing the CPU time of the spatially hybrid approaches with a simulation with fully kinetic neutrals, approach (i) leads to a higher speed-up than approach (ii) especially for cases where the majority of ions and atoms are thermally recycled as molecules. However, the accuracy of approach (i) is limited compared with approach (ii). Therefore, we use in this paper a micro–macro approach for Equation (7) instead of a purely fluid description to increase the accuracy of approach (i) without the need for a fully kinetic description for atoms resulting from molecular dissociation.

The micro–macro distribution  $f_a^{\text{mM}}(\mathbf{r}, \mathbf{v})$  consists of a fluid/equilibrium (macro) and kinetic correction (micro) part:

$$f_a^{\text{mM}}(\mathbf{r}, \mathbf{v}) = f_a^{\text{f}}(\mathbf{r}, \mathbf{v}) + f_a^{\delta}(\mathbf{r}, \mathbf{v}), \quad (8)$$

where the expression of  $f_a^{\text{f}}$  corresponds to the chosen fluid model (see Section 3.2.1). In the micro–macro approach, the macroscopic properties for which fluid moments are solved follow entirely from the corresponding fluid equations,<sup>[16]</sup> which implies

$$\int_{\mathbf{v}} \boldsymbol{\mu}(\mathbf{v}) f_a^{\delta}(\mathbf{r}, \mathbf{v}) d\mathbf{v} \equiv 0, \quad (9)$$

with  $\boldsymbol{\mu}(\mathbf{v})$  all moments that are present in the fluid model. Condition (9) implies that there is no need for a fluid/kinetic detection criterion to determine which regions are more fluid or kinetic and consequently it eliminates the need to decide whether an atom from dissociation is fluid or kinetic. Condition (9) is imposed to derive the micro–macro equations in a continuous setting in Sections 3.2.1 and 3.2.2. However, when representing the kinetic correction  $f_a^{\delta}(\mathbf{r}, \mathbf{v})$  by a finite amount of MC particles, Condition (9) is violated. This can be resolved by adding a projection step,<sup>[17]</sup> but integration of the projection step in SOLPS-ITER is still future research.

#### 3.2.1 | Macro/fluid equations

The macro/fluid equations are obtained by taking moments of Equation (7) using Equation (8) and Condition (9). The fluid atom model in SOLPS-ITER consists of a continuity and parallel momentum equation ( $\boldsymbol{\mu}(\mathbf{v}) = [1 \quad mv_{\parallel}]^T$ , with  $v_{\parallel}$  the particle-velocity component parallel to the magnetic field), assuming that the fluid atoms have the ion temperature ( $T_i$ ):

$$\nabla \cdot (n_a \mathbf{V}_a) = S_{n_a}, \quad (10)$$

$$\nabla \cdot (mn_a u_{a\parallel} \mathbf{V}_a - \eta_a \nabla u_{a\parallel}) + \left[ \nabla \cdot \left( \int_{\mathbf{v}} m \mathbf{v} \mathbf{v} f_a^{\delta}(\mathbf{v}) d\mathbf{v} \right) \right]_{\parallel} = -\nabla_{\parallel} (n_a T_i) + S_{mu_{a\parallel}} + S_{cf}, \quad (11)$$

where  $\mathbf{V}_a$  refers to atom fluid velocity vector,  $u_{a\parallel}$  refers to parallel component of the atom fluid velocity,  $\eta_a$  refers to fluid atom viscosity, and  $S_{cf}$  is a term that accounts for curvature contributions due to the toroidal geometry. Equation (11) is similar to the ion parallel momentum equation of B2.5.<sup>[18]</sup> The sources  $S_{n_a}$  and  $S_{mu_{a\parallel}}$  follow from

$$\begin{bmatrix} S_{n_a} & S_{mu_{a\parallel}} \end{bmatrix}^T = \int_{\mathbf{v}} \boldsymbol{\mu}(\mathbf{v}) (S_a^{\text{mM}}(\mathbf{v}) + Q_a (f_a^{\text{mM}}(\mathbf{v}))) d\mathbf{v}. \quad (12)$$

The transport in the radial ( $r$ ) and diamagnetic ( $\perp$ ) directions follows from reduced momentum equations:

$$[n_a \mathbf{V}_a]_{r,\perp} = -\frac{1}{m (n_i K_{cx,m} + n_e K_i)} \left( \nabla_{r,\perp} (n_a T_i) + \left[ \nabla \cdot \int_{\mathbf{v}} m \mathbf{v} \mathbf{v} f_a^{\delta}(\mathbf{v}) d\mathbf{v} \right]_{r,\perp} \right). \quad (13)$$

In the fluid model, improved expressions are used for the transport coefficients and boundary conditions to be as consistent as possible with the underlying kinetic description.<sup>[19,20]</sup> In contrast to a purely fluid neutral model, there appear

kinetic correction terms in Equation (11) and (13) to correct for the assumptions made when closing the fluid moment equations.

In the micro model (Section 3.2.2), an expression for  $f_a^f$  is required. The fluid stress tensor in Equation (11) corrects for first-order non-Maxwellian effects. Hence, the distribution  $f_a^f$  fully consistent with Equations (10)–(13) deviates from a perfect Maxwellian distribution. However, in this paper, we still assume a perfect drifting Maxwellian for  $f_a^f$ , that is,

$$f_a^f(\mathbf{v}) \approx n_a \left( \frac{m}{2\pi T_i} \right)^{3/2} \exp \left( -\frac{m}{2T_i} \|\mathbf{v} - u_{a\parallel} \mathbf{e}_{\parallel}\|^2 \right), \quad (14)$$

where  $\mathbf{e}_{\parallel}$  is unit vector parallel to the magnetic field. Equation (14) leads to remaining modelling error, but significantly simplifies the implementation of the micro part in EIRENE.

When running SOLPS-ITER with fluid neutral model, one usually solves the sum of the ion and neutral energy equations assuming an equal temperature for all species. For the combined spatially–micro–macro hybrid approach of this paper, however, we exclude the neutral energy contributions to obtain an energy equation exclusively for the ion species. Consequently, there is an explicit correction for neutral-ion temperature differences in the ion energy source and there is no introduction of an additional modelling error in Equation (14) when neglecting corrections due to fluid atom heat conduction. The fluid atom temperature ( $T_a$ ) used in the ion energy source is given by

$$T_a = T_i + \frac{1}{n_a} \int_{\mathbf{v}} \frac{m}{3} \|\mathbf{v}\|^2 f_a^{\delta}(\mathbf{v}) d\mathbf{v}. \quad (15)$$

### 3.2.2 | Micro/kinetic correction equation

The kinetic correction terms in Equations (10)–(15) follow from an MC simulation of the micro equation, which is obtained by plugging Equation (8) in Equation (7). After re-arranging the terms, this gives

$$\mathbf{v} \cdot \nabla f_a^{\delta}(\mathbf{r}, \mathbf{v}) = S_a^{\text{mM}}(\mathbf{r}, \mathbf{v}) + Q_a(f_a^f(\mathbf{r}, \mathbf{v})) - \mathbf{v} \cdot \nabla f_a^f(\mathbf{r}, \mathbf{v}) + Q_a(f_a^{\delta}(\mathbf{r}, \mathbf{v})). \quad (16)$$

The first three terms on the right-hand side of Equation (16) are the sources of kinetic correction atoms. The sum corresponds to the residual of the kinetic equation (Equation (7)) assuming that  $f_a^{\text{mM}} \equiv f_a^f$ , that is, the error from the fluid approximation. With the help of Equation (3), the collision term becomes

$$Q_a(f_a^{\delta}(\mathbf{v})) = - (n_e K_i + n_i K_{\text{cx,m}}) f_a^{\delta}(\mathbf{v}). \quad (17)$$

Due to Condition (9), the zeroth-order moment of  $f_a^{\delta}$  is zero and there is no density in the kinetic correction part. This zero kinetic correction density makes that charge-exchange scattering collisions have been transformed into absorption events, which leads to a significant reduction in CPU cost of the MC part (see Section 4.4).

If Equation (3) is not valid, then it is no longer possible to make the charge-exchange collisions purely absorbing in the micro model. However, the exact charge-exchange rate coefficient  $K_{\text{cx}}$  can still be written as

$$K_{\text{cx}} = K_{\text{cx,m}} + \delta K_{\text{cx}}, \quad (18)$$

where  $\delta K_{\text{cx}}$  is a correction for the momentum-linearized approximation. Only  $\delta K_{\text{cx}}$  will introduce scattering collisions in the micro model, whereas the bulk of charge-exchange events is contained in the purely absorbing  $K_{\text{cx,m}}$ . Figure 2 shows for an atom the ratio of the probability of scattering for the micro model (due to the charge-exchange correction term),  $P_s^{\text{m}}$ , and the probability of scattering for the fully kinetic approach (due to the total charge-exchange cross-section),  $P_s^{\text{k}}$ , as a function of the atom kinetic energy. The vertical lines in Figure 2 correspond to an energy of  $4T_i$ . If the atoms have a Maxwellian distribution, 95% of the particles have an energy smaller than this value. For energies lower than  $4T_i$ ,  $P_s^{\text{m}}/P_s^{\text{k}}$  becomes significantly smaller than one. Hence, even if the approximation of Equation (3) is violated, the scattering contribution in the micro MC simulation remains small, which immediately translates in a speed-up. In this paper, we have not yet implemented the corrections due to  $\delta K_{\text{cx}}$ , because the influence of the momentum-linearized assumption on the plasma state is limited for our cases (see Section 4.2).

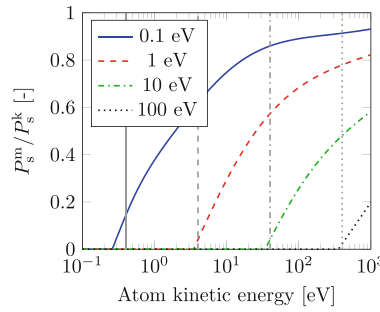


**FIGURE 2** Ratio of the probability of a scattering event for the micro and fully kinetic MC simulations based on the AMJUEL reaction data.<sup>[21]</sup> The legend indicates the different values for  $T_i$ . We assume  $n_e = n_i$  and  $T_e = T_i$

### 3.3 | Boundary conditions and coupling of the fluid and kinetic parts

At the boundaries of the fluid grid (divertor targets and micro–macro–kinetic interfaces), we impose fluid fluxes as boundary conditions for the macro equations, given by

$$\begin{aligned} \Gamma_\mu(\mathbf{r}) = & \int_{\mathbf{v} \cdot \mathbf{v} \leq 0} \mu(\mathbf{v}) f_a^f(\mathbf{r}, \mathbf{v}) (\mathbf{v} \cdot \mathbf{v}) d\mathbf{v} \\ & - \int_{\mathbf{v} \cdot \mathbf{v} > 0} \mu(\mathbf{v}) \left( \int_{\mathbf{v}' \cdot \mathbf{v} \leq 0} R_f(\mathbf{r}; \mathbf{v}' \rightarrow \mathbf{v}) (f_a^f(\mathbf{r}, \mathbf{v}') + f_i(\mathbf{r}, \mathbf{v}')) (\mathbf{v}' \cdot \mathbf{v}) d\mathbf{v}' \right) d\mathbf{v}, \text{ for } \mathbf{r} \in \partial D, \end{aligned} \quad (19)$$

with  $\partial D$  the boundary of the fluid domain,  $\mu(\mathbf{v})$  corresponding to the particular fluid moments, and  $\int_{\mathbf{v} \cdot \mathbf{v} \leq 0} \dots d\mathbf{v}$  and  $\int_{\mathbf{v} \cdot \mathbf{v} > 0}$  the integral over the incident and reflected velocity space, respectively ( $\mathbf{v}$  corresponds to the boundary unit normal pointing into the fluid domain). As before,  $f_a^f(\mathbf{r}, \mathbf{v})$  is approximated by Equation (14). The first term on the right-hand side of Equation (19) consists of the contribution of fluid atoms hitting a boundary of the fluid grid and the second term contains the recycled contributions, with  $R_f(\mathbf{r}; \mathbf{v}' \rightarrow \mathbf{v})$  the probability that an incident particle is recycled as a fluid atom multiplied by the reflection-velocity distribution, determined by, for example, the TRIM database.<sup>[15]</sup> At the divertor targets,  $\int_{\mathbf{v} \cdot \mathbf{v} > 0} R_f(\mathbf{r}; \mathbf{v}' \rightarrow \mathbf{v}) d\mathbf{v} = 1 - R_t(\mathbf{r}; \mathbf{v}')$ , with  $R_t(\mathbf{r}; \mathbf{v}')$  the probability that a particle is thermally released as a molecule. At the micro–macro – kinetic interfaces,  $R_f(\mathbf{r}; \mathbf{v}' \rightarrow \mathbf{v}) \equiv 0$  due to the fully kinetic treatment of the strata at the micro–macro – kinetic interfaces.

It should be noted that we use  $f_a^f(\mathbf{r}, \mathbf{v})$  in Equation (19) instead of the complete micro–macro distribution  $f_a^{\text{mM}}(\mathbf{r}, \mathbf{v})$ . When using  $f_a^{\text{mM}}(\mathbf{r}, \mathbf{v})$ , also MC particles of the micro equation would have to be transferred to fully kinetic molecules or fully kinetic atoms sent into the void regions. The re-conversion of the absorption-dominated collision term of Equation (17) to the original absorption-scattering term of Equation (3) would lead to a significant increase in computational cost. In addition, the treatment of the combination of positively and negatively weighted micro particles with a fully kinetic approach leads to a large bias and requires a significant increase of required MC histories. This so-called finite-sampling bias, which is studied in detail for coupled fluid-kinetic plasma edge simulations<sup>[22]</sup> and specifically for the micro–macro approach,<sup>[17]</sup> originates from the non-linear coupling between a deterministic system (the fluid equations) and a stochastic system (the kinetic equations) represented by a finite amount of particles. In the asymptotic regime, the finite-sampling bias typically scales with  $1/N$ , with  $N$  the amount of MC histories. In Section 4.3, we illustrate that using  $f_a^{\text{mM}}$  instead of  $f_a^f$  in Equation (19) demands for a drastic increase in the required amount of MC histories. Hence, we use  $f_a^f(\mathbf{r}, \mathbf{v})$  for both the fluid boundary conditions (Equation [19]) and to sample fully kinetic particles at the micro–macro – kinetic interfaces (second contribution of  $S_a^k$  in Section 3.1), which leads to an additional modelling error.

### 3.4 | Impact of neutral–neutral collisions on the hybrid model

As mentioned in Section 2, neutral–neutral collisions are not yet included in the collision term of Equation (2). In this section, we briefly discuss the impact of neutral–neutral collisions on the model equations. The implementation and a detailed study of the influence of neutral–neutral collisions on the accuracy and performance of the hybrid model are kept

as future research. For the fully kinetic model for neutrals in the plasma edge, non-linear neutral–neutral collisions are typically incorporated by means of a BGK approximation, where neutrals interact with the neutral solution of the previous iteration on the plasma state.<sup>[23]</sup> To this end, macroscopic neutral properties (density, flow velocity, and temperature) are saved and used in the next iteration as a neutral background. With the BGK approximation, the fully kinetic collision term for elastic atom–atom collisions can be written as

$$Q_a^{\text{el,a}}(f_a(\mathbf{v})) = n_a K_{\text{el}}^{\text{aa}} \left( n_a \tilde{M}(\mathbf{v}; \mathbf{V}_a, T_a) - f_a(\mathbf{v}) \right), \quad (20)$$

where  $K_{\text{el}}^{\text{aa}}$  is the atom–atom collision rate coefficient and  $\tilde{M}(\mathbf{v}; \mathbf{V}_a, T_a)$  is a normalized drifting Maxwellian distribution.

The spatial decomposition step from Section 3.1 remains unchanged except for an additional collision contribution in the right-hand side of Equation (6), given by

$$Q_a^{\text{el,a}}(f_a^{\text{k}}(\mathbf{v})) = n_a^{\text{t}} K_{\text{el}}^{\text{aa}} \left( n_a^{\text{k}} \tilde{M}(\mathbf{v}; \mathbf{V}_a^{\text{t}}, T_a^{\text{t}}) - f_a^{\text{k}}(\mathbf{v}) \right), \quad (21)$$

with the macroscopic properties of the total distribution (fully kinetic and micro–macro) given by

$$n_a^{\text{t}} \triangleq n_a + \int_{\mathbf{v}} f_a^{\text{k}}(\mathbf{v}) d\mathbf{v}, \quad (22)$$

$$\mathbf{V}_a^{\text{t}} \triangleq \frac{1}{n_a^{\text{t}}} \left( n_a \mathbf{V}_a + \int_{\mathbf{v}} \mathbf{v} f_a^{\text{k}}(\mathbf{v}) d\mathbf{v} \right), \quad (23)$$

$$T_a^{\text{t}} \triangleq \frac{1}{n_a^{\text{t}}} \left( n_a T_a + \int_{\mathbf{v}} \frac{m}{3} \|\mathbf{v}\|^2 f_a^{\text{k}}(\mathbf{v}) d\mathbf{v} + \frac{m}{3} \left( n_a \|\mathbf{V}_a\|^2 - n_a^{\text{t}} \|\mathbf{V}_a^{\text{t}}\|^2 \right) \right). \quad (24)$$

Due to Condition (9), the density  $n_a$  and velocity  $\mathbf{V}_a$  follow from the fluid solution (Equations [10], [11], and [13]). The only kinetic correction contribution from  $f_a^{\delta}$  is contained in the temperature  $T_a$ , given by Equation (15). Hence, the fully kinetic population interacts to a large extent with the fluid atom background, which is expected to improve the statistics compared with a fully kinetic approach in the entire domain.

After the micro–macro decomposition, the macro equations (Equation [10], [11], and [13]) remain unchanged, except for the incorporation of the neutral–neutral collisions in the transport coefficients and an additional friction term due to elastic collisions between the fluid and fully kinetic neutrals. The micro equation gets an additional source contribution from the fluid population in the right-hand side of Equation (16), given by

$$Q_a^{\text{el,a}}(f_a^{\text{f}}(\mathbf{v})) = n_a^{\text{t}} K_{\text{el}}^{\text{aa}} \left( n_a \tilde{M}(\mathbf{v}; \mathbf{V}_a^{\text{t}}, T_a^{\text{t}}) - f_a^{\text{f}}(\mathbf{v}) \right). \quad (25)$$

The collision term of Equation (17) also gets an additional contribution:

$$Q_a^{\text{el,a}}(f_a^{\delta}(\mathbf{v})) = -n_a^{\text{t}} K_{\text{el}}^{\text{aa}} f_a^{\delta}(\mathbf{v}). \quad (26)$$

Again, due to Condition (9) and the BGK approximation (Equation [20]), neutral–neutral collisions are transformed to pure absorption events in the micro equation, leading to a reduction of the average CPU time per MC particle.

## 4 | RESULTS

### 4.1 | Description of the test case and overview of the models

The methods are tested for the purely deuterium JET ITER-like wall L-mode cases (discharge 81,472) in the absence of electromagnetic drifts, as described.<sup>[6]</sup> The upstream conditions are set by imposing a constant ion/electron density  $n_{\text{core}}$  at the core boundary (see Figure 1). We consider a high-recycling and partially detached case with  $n_{\text{core}} = 2.0 \cdot 10^{19} \text{ m}^{-3}$  and  $n_{\text{core}} = 4.0 \cdot 10^{19} \text{ m}^{-3}$ , respectively.

**TABLE 1** Overview of the different neutral models, indicating the treatment of the different types of particles

Model	Atoms from volumetric recombination	Atoms from target surface recombination	Atoms at plasma-void interfaces	Atoms from molecular dissociation	Molecules
Kinetic (Kin)	Kinetic	Kinetic	Kinetic	Kinetic	Kinetic
Fluid (Fl)	Fluid	Fluid	Fluid (no voids)	—	3 eV atoms
Spatially hybrid 1 (Sp1)	Fluid	Fluid	Kinetic	Fluid	Kinetic
Spatially hybrid 2 (Sp2)	Fluid	Fluid	Kinetic	Kinetic	Kinetic
Combined spatially – micro–macro (Sp-mM)	Micro–macro	Micro–macro	Kinetic	Micro–macro	Kinetic

Besides a comparison between simulations with fully kinetic neutrals and the newly developed combined spatially–micro–macro approach, there is also a comparison with simulations with a purely fluid neutral model and with the original spatially hybrid approach from Reference [6]. Table 1 gives an overview of the different neutral models with the acronyms used in upcoming sections. For simulations with a purely fluid neutral model (Fl), the void regions are omitted and the recycling model (TRIM<sup>[15]</sup>) for incident neutrals is already applied at the plasma-void interfaces. When a particle is thermally recycled as a molecule, it is assumed that the molecule immediately dissociates into atoms with an energy of 3 eV according to the Franck–Condon dissociation process. Consequently, there is no explicit treatment of molecules for simulations with a purely fluid neutral model.

## 4.2 | Divertor target profiles

All hybrid approaches (Sp1, Sp2, and Sp-mM) significantly reduce the discrepancies between a simulation with fully kinetic neutrals (Kin) and a simulation with a purely fluid neutral model (Fl). However, the fluid treatment of atoms resulting from molecular dissociation in Sp1 gives a lower accuracy than the kinetic and micro–macro treatment in Sp2 and Sp-mM, respectively (see Figure 3). Sp2 and Sp-mM give approximately the same order of accuracy, but there is a significant reduction in average CPU time per MC particle due to the micro–macro approach in Sp-mM (see Section 4.4). The inexact micro–macro decomposition by assuming a perfect drifting Maxwellian for  $f_a^f$  (see Equation [14]) and at the plasma-void interfaces (see Section 3.3) gives a remaining modelling error for Sp-mM compared with Kin. In fact, the approximate expression for the charge-exchange collision term (Equation [3]) also contributes to hybrid-kinetic discrepancies, but the influence on the plasma state is small for the cases of this paper, which we conclude by comparing the blue solid and dashed lines in Figure 3. From the simulation with fully kinetic neutrals, we conclude that Equation (3) is valid for our cases and we use the approximate collision term also for the simulations with fluid and hybrid neutrals.

Similar to previous observations from EDGE2D-EIRENE simulations for these JET L-mode cases,<sup>[24]</sup> we conclude that the outer divertor detaches earlier than the inner divertor. Even when including electromagnetic drifts in the simulations, the inner divertor detaches earlier in the experiments than predicted by the simulations. This simulation–experiment discrepancy is material for future research.

To quantify the contribution of the kinetic correction terms in Equations (10), (11), and (13), Figure 4 compares the fluid and kinetic contributions ( $p_a^f \stackrel{\Delta}{=} n_a T_i$  and  $p_a^\delta \stackrel{\Delta}{=} \int_{\mathbf{v}} \frac{m}{3} \|\mathbf{v}\|^2 f_a^\delta(\mathbf{v}) d\mathbf{v}$ , respectively) to the atomic pressure of the micro–macro part ( $p_a^f + p_a^\delta$ ) for the Sp-mM converged state. Due to the larger charge-exchange mean-free-path lengths for the high-recycling case ( $n_{\text{core}} = 2.0 \cdot 10^{19} \text{ m}^{-3}$ ), the error from the fluid atom solution is larger than for the detached case ( $n_{\text{core}} = 4.0 \cdot 10^{19} \text{ m}^{-3}$ ). The inaccuracy of the fluid atom model directly translates to a larger relative contribution of the kinetic correction  $p_a^\delta$  to the total atomic pressure, as can be clearly seen by comparing Figure 4a,b with Figure 4c,d. For  $n_{\text{core}} = 2.0 \cdot 10^{19} \text{ m}^{-3}$ , the maximum fluid-kinetic discrepancy is reached in the vicinity of the step between tile 5 and 6 at the outer target, as can be seen by comparing the green solid (Fl) and red dashed (Sp1) lines with the blue (Kin) lines in Figure 3b in the grey shaded area. The fluid solution overpredicts the neutral atom temperature in the region of the step, which is compensated by a negative kinetic correction on the atom pressure (see Figure 4b).

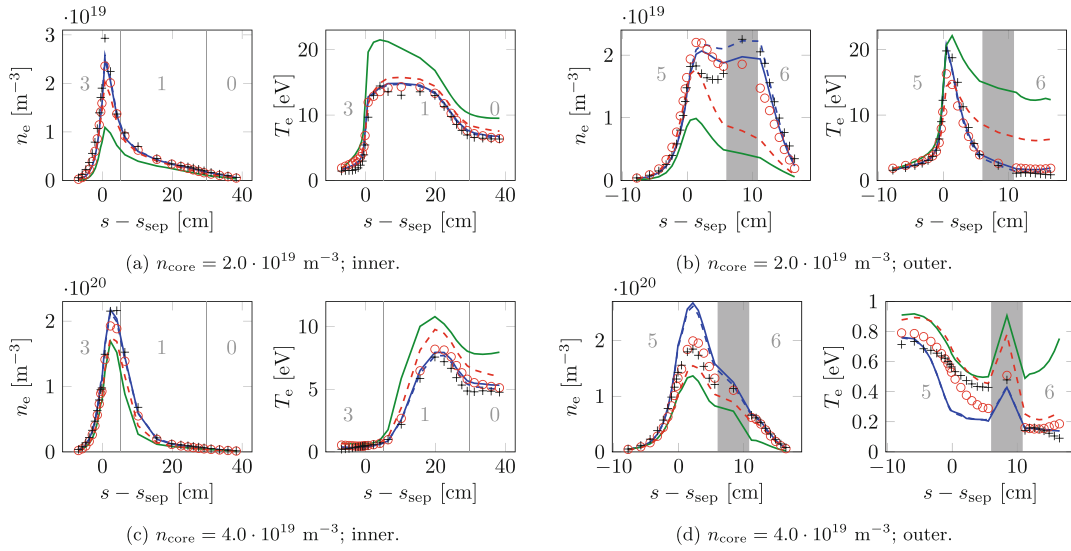


**FIGURE 3** Divertor target plasma profiles as a function of the strike-point distance along the target plate  $s - s_{\text{sep}}$ : Kin (blue), FI (green), Sp1 (red dashed line), Sp2 (red circular marks), and Sp-mM (black pluses) (see Table 1 for the meaning of the acronyms). Equation (2) is used for the collision term for the blue solid lines, whereas Equation (3) is used for the blue dashed lines. The grey lines and numbers indicate the different tile positions (see Figure 1), with the grey shaded area corresponding to the step between tile 5 and 6

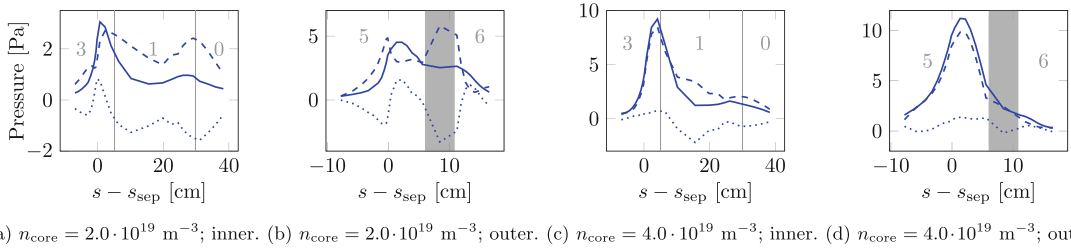


**FIGURE 4** Atomic pressure at the divertor targets: fluid part  $p_a^f$  (dashed), kinetic correction part  $p_a^\delta$  (dotted), and total  $p_a^f + p_a^\delta$  (solid). The grey lines and numbers indicate the different tile positions (see Figure 1), with the grey shaded area corresponding to the step between tiles 5 and 6

The largest remaining discrepancies between the hybrid approaches Sp2 and Sp-mM and the simulation with fully kinetic neutrals (Kin) occur for the detached outer divertor (see Figure 3). For detached conditions, the dynamics of the molecules play a more crucial role than for a high-recycling case. The solutions for the molecules in the hybrid approaches are to a large extent determined by the coupling boundary between the micro-macro and fully kinetic parts (Equation (19)). As explained in Section 3.3, we use the approximate fluid atom distribution  $f_a^f$  instead of the micro-macro distribution  $f_a^{\text{mM}}$  at the boundaries, which leads to a modelling error. As future work, we intend to improve the expression for the distribution at the boundaries to further increase the resulting accuracy of the hybrid model in detached conditions.

### 4.3 | Effect of using the micro-macro distribution at the micro-macro-fully kinetic interfaces

As discussed at the end of Section 3.3, the use of the more accurate micro-macro distribution  $f_a^{\text{mM}}$  instead of the fluid atom distribution  $f_a^f$  in the interface boundary condition (Equation [19]) leads to a much larger finite-sampling bias. We illustrate this for simulations with exclusively atoms and no void regions, that is, the same settings as for the purely fluid neutral model described in Section 4.1. Particles hitting the plasma-void interfaces (see Figure 1) are reflected

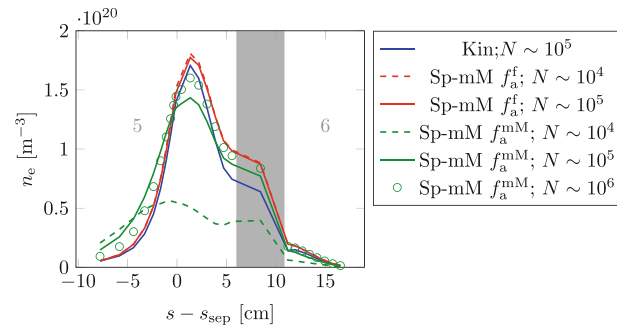


**FIGURE 5** Electron density at the outer target when varying the amount of MC histories  $N$  and the distribution in Equation (19) (atoms only, no voids,  $n_{\text{core}} = 4.0 \cdot 10^{19} \text{ m}^{-3}$ ): using Equation (19) at the interface (green) and replacing  $f_a^f$  by  $f_a^{\text{mM}}$  in Equation (19) (red)

**TABLE 2** Ratio of the CPU time for a simulation with fully kinetic neutrals and the different hybrid neutral models for the same amount of MC particles (see Table 1 for the meaning of the acronyms)

Model	$n_{\text{core}} = 2.0 \cdot 10^{19} \text{ m}^{-3}$	$n_{\text{core}} = 4.0 \cdot 10^{19} \text{ m}^{-3}$
Sp1	1.72	2.15
Sp2	0.97	1.08
Sp-mM	3.33	11.05

and kinetic correction particles from  $f_a^\delta$  are transferred to the fully kinetic population  $f_a^k$ . By varying the total amount of MC histories, we conclude that the minimum amount of particles to get physics relevant results becomes much larger when replacing  $f_a^f$  by  $f_a^{\text{mM}}$  in Equation (19) ( $N \sim 10^4$  is unacceptable as illustrated by the green dashed line in Figure 5).

#### 4.4 | Performance

When using the same number of particles for the different hybrid models as for a simulation with fully kinetic neutrals, there is a significant reduction of the CPU time for the newly developed combined spatially–micro–macro approach (Sp-mM) (Table 2). The fraction of particles assigned to each stratum is based on the source strength of the stratum. The speed-up compared with Kin for the purely spatially hybrid models (Sp1 and Sp2) is limited, with even an increase in CPU time for Sp2 at  $n_{\text{core}} = 2.0 \cdot 10^{19} \text{ m}^{-3}$ . Due to the redistribution of the particles, more particles are assigned to the molecular strata at the targets, for which the average CPU time is higher. In Reference [6], however, it is clearly shown that the purely spatially hybrid approaches reduce the statistical error on a certain quantity of interest with, on average, a factor 3. This allows to reduce the total amount of MC particles. The effect of the transformation of the collision term to Equation (17) is visible in the CPU-time reductions for Sp-mM. The efficiency of the micro–macro approach increases when moving to more charge-exchange dominated regimes by increasing the upstream density due to the transformation of a charge-exchange event to an absorption event. A thorough statistical analysis will be addressed in future publications.

## 5 | CONCLUSIONS AND OUTLOOK

By combining the spatially hybrid approach from Reference [6] with the micro–macro approach from Reference [8], we add a kinetic correction on top of the fluid part. This automatic correction is especially successful for the treatment of atoms resulting from molecular dissociation, which were recommended to be treated as a fluid in the original spatially hybrid approach to reduce the computational cost, at the expense of accuracy. The newly developed hybrid approach is able to predict the plasma target profiles within 30% of accuracy compared with a simulation with fully kinetic neutrals, but with a reduction of average CPU time for a single MC particle with approximately a factor 3 for a low-density

(high-recycling) case and a factor 11 for a high-density (partially detached) case. By also using the micro–macro approach for atoms from molecular dissociation, it is no longer needed to determine in advance if an atom from dissociation has to be treated as a fluid or kinetically.

As future work, it is recommended to increase the computational performance of the method. Due to the transformation of the typically charge-exchange dominated fully kinetic equation to the absorption-dominated micro equation, the MC estimators can be improved to limit the statistical error.<sup>[25]</sup> In addition, the statistical error can be further reduced by exploring methods to combine positively and negatively weighted particles. Finally, the maximum achievable speed-up is still limited due to a fully kinetic MC treatment of the molecules. It is worth investigating if a fluid model becomes also valid for molecules (as implemented in the UEDGE code<sup>[26]</sup>) and if the hybrid approach can be extended for this purpose.

## ACKNOWLEDGEMENTS

This work has been carried out within the framework of the EUROfusion Consortium and has received funding from the Euratom research and training programme 2014–2018 and 2019–2020 under grant agreement No 633053. The views and opinions expressed herein do not necessarily reflect those of the European Commission.

## CONFLICT OF INTEREST

The authors declare no potential conflict of interests.

## AUTHOR CONTRIBUTIONS

Niels Horsten: Conceptualization; Formal analysis; Investigation; Methodology; Software; Validation; Visualization; Writing – Original Draft. Mathias Groth: Conceptualization; Project Administration; Supervision; Writing – Review and Editing. Wouter Dekeyser: Data Curation; Methodology; Software; Writing – Review and Editing. Wim Van Uytven: Methodology; Software; Writing – Review and Editing. Stefano Carli: Data Curation; Software; Writing – Review and Editing.

## DATA AVAILABILITY STATEMENT

The data that support the findings of this study are available from the corresponding author upon reasonable request. The simulations are stored on the IPP Garching cluster in the directory /toks/work/nhorst/SOLPS us/solps-iter/runs/PET2021.

## REFERENCES

- [1] S. Braginskii, *Rev. Plasma Phys.* **1965**, *1*, 205.
- [2] D. Reiter, M. Baelmans, P. Börner, *Fusion Sci. Technol.* **2005**, *47*(2), 172.
- [3] D. Knoll, P. McHugh, S. Krasheninnikov, D. Sigmar, *Phys. Plasmas* **1996**, *3*(1), 293.
- [4] M. Rensink, L. Lodestro, G. Porter, T. Rognlien, D. Coster, *Contrib. Plasma Physics* **1998**, *38*(1–2), 325.
- [5] M. Furubayashi, K. Hoshino, M. Toma, A. Hatayama, D. Coster, R. Schneider, X. Bonnin, H. Kawashima, N. Asakura, Y. Suzuki, *J. Nucl. Mater.* **2009**, *390*, 295.
- [6] N. Horsten, M. Groth, M. Blommaert, W. Dekeyser, I. P. Pérez, S. Wiesen, J. Contributors, *Nucl. Mater. Energy* **2021**, *27*, 100969.
- [7] M. Blommaert, N. Horsten, P. Börner, W. Dekeyser, *Nucl. Mater. Energy* **2019**, *19*, 28.
- [8] N. Horsten, W. Dekeyser, M. Blommaert, G. Samaey, M. Baelmans, *Contrib. Plasma Physics* **2020**, *60*(5–6), e201900132.
- [9] W. Dekeyser, P. Boerner, S. Voskoboynikov, V. Rozhansky, I. Senichenkov, L. Kaveeva, I. Veselova, E. Vekshina, X. Bonnin, R. Pitts, M. Baelmans, *Nucl. Mater. Energy* **2021**, *27*, 100999.
- [10] W. Dekeyser, X. Bonnin, S. Ligo, R. Pitts, B. LaBombard, *Nucl. Mater. Energy* **2019**, *18*, 125.
- [11] N. Horsten, W. Dekeyser, G. Samaey, M. Baelmans, *Nucl. Mater. Energy* **2017**, *12*, 869.
- [12] H. Bufferand, B. Bensiali, J. Bucalossi, G. Ciraolo, P. Genesio, P. Ghendrih, Y. Marandet, A. Paredes, F. Schwander, E. Serre, P. Tamain, *J. Nucl. Mater.* **2013**, *438*, S445.
- [13] M. Valentinuzzi, Y. Marandet, H. Bufferand, G. Ciraolo, P. Tamain, *Nucl. Mater. Energy* **2019**, *18*, 41.
- [14] W. Van Uytven, W. Dekeyser, M. Blommaert, N. Horsten, Y. Marandet, M. Baelmans, accepted for *Contrib. Plasma Physics*.
- [15] D. Reiter, *The EIRENE code user manual.* **2009**.
- [16] A. Crestetto, N. Crouseilles, M. Lemou, *Kinet. Relat. Models* **2012**, *5*(4), 787.
- [17] N. Horsten, G. Samaey, M. Baelmans, *J. Comput. Phys.* **2020**, *409*, 109308.
- [18] V. Rozhansky, S. Voskoboynikov, E. Kaveeva, D. Coster, R. Schneider, *Nucl. Fusion* **2001**, *41*(4), 387.
- [19] N. Horsten, G. Samaey, M. Baelmans, *Nucl. Fusion* **2017**, *57*(11), 116043.
- [20] M. Blommaert, W. Dekeyser, N. Horsten, P. Börner, M. Baelmans, *Contrib. Plasma Physics* **2018**, *58*(6–8), 718.

- [21] D. Reiter. The data file AMJUEL: Additional atomic and molecular data for EIRENE, Technical report, FZ Juelich, **2000**.
- [22] K. Ghooos, W. Dekeyser, G. Samaey, P. Börner, M. Baelmans, *J. Comput. Phys.* **2016**, 322, 162.
- [23] D. Reiter, C. May, M. Baelmans, P. Börner, *J. Nucl. Mater.* **1997**, 241, 342.
- [24] M. Groth, S. Brezinsek, M. Clever, A. Huber, K. D. Lawson, A. G. Meigs, M. F. Stamp, J. Svensson, S. Wiesen, P. Belo, M. Brix, J. W. Coenen, G. Corrigan, C. Giroud, C. Guillemaut, D. Harting, S. Jachmich, M. Lehnen, C. F. Maggi, C. Marchetto, S. Marsen, C. Silva, G. J. van Rooij, and the JET contributors, 25th IAEA Fusion Energy Conf. (FEC 2014). **2014**.
- [25] B. Mortier, M. Baelmans, G. Samaey, in Proceedings of Int. Conf. on Mathematics & Computational Methods Applied to Nuclear Science & Engineering. **2017**.
- [26] A. Holm, T. Rognlien, W. Meyer, *Contrib. Plasma Physics* **2020**, 60(5–6), e201900150.

**How to cite this article:** N. Horsten, M. Groth, W. Dekeyser, W. Van Uytven, S. Carli, *Contributions to Plasma Physics* **2022**, 62(5-6), e202100188. <https://doi.org/10.1002/ctpp.202100188>